


RESEARCH ARTICLE OPEN ACCESS

Analytical Solution for Railway Transition Zones With Abrupt Changes in Elastic Stiffness

Josiah Murray¹ | Michael H. Meylan¹ | Trung Ngo² | Ngamta Thamwattana¹  | Buddhima Indraratna²

¹School of Information and Physical Sciences, University of Newcastle, Callaghan, New South Wales, Australia | ²Transport Research Centre, School of Civil and Environmental Engineering, University of Technology Sydney, New South Wales, Australia

Correspondence: Ngamta Thamwattana (natalie.thamwattana@newcastle.edu.au)

Received: 22 December 2024 | **Revised:** 12 March 2025 | **Accepted:** 13 March 2025

Funding: This work was supported by Australian Research Council DP220102862.

Keywords: closed-form solutions | elastic stiffness | Euler-Bernoulli beam equation | railway transition zones

ABSTRACT

Transition zones in railway systems, where properties of the track foundation change abruptly, are known to increase dynamic loads, track deterioration, and passenger discomfort. As such, it is of particular importance to study railway transition zones with abrupt changes in foundation properties to minimize these railway problems. This paper presents a closed-form solution for the long-term deformation of an Euler-Bernoulli beam on an elastic foundation with multiple abrupt changes in foundation stiffness and under multiple applied stationary point loads. The solutions are obtained by dividing the beam into segments and applying the method of undetermined coefficients. This exact analytical solution constitutes an improvement upon an approximate solution, which is presented in the literature as a recent method for modeling rail infrastructure at transition zones. A limitation of the approximate solution is its inability to account for the changed behavior of the beam close to a transition zone. The closed-form solution overcomes this limitation and can be used to assess the suitability of the approximate solution.

1 | Introduction

The need for increasingly efficient railway systems, driven in part by rising populations, is ever present and continuously driving innovation and improvement [1]. This is no less true for Australia and its approximately 30,000km long rail network [2]. In some areas, Australia is playing a leading role, for instance with heavy haul rail networks [3] but is lacking in other areas, such as the uptake of high-speed networks (Australia's trains being limited to a maximum of 160km/h) [4]. In either case, this motivates research into methods for analyzing and improving railway infrastructure.

Infinite beam-on-elastic-foundation models have been used to study railway tracks since at least 1888 [5], having also been

applied in a variety of other fields [6–8]. In classical formulations, the foundation is assumed to be homogeneous under the entire length of the beam, however, in practice this is frequently an oversimplification and more recent work has also considered inhomogeneous foundations. A rail line, for instance, may experience an abrupt change in foundation stiffness when moving between a soil subgrade and a concrete foundation associated with a bridge or culvert. Inhomogeneities such as these are commonly referred to as “transition zones” [7, 9–11]. Plastic deformations accumulate at different rates across the transition zone creating differential settlements, which increase dynamic loads on the track, track deterioration, and passenger discomfort, thereby necessitating more frequent maintenance [7, 12]. Research into approaches for mitigating the differential settlement across transition zones is ongoing and motivates a better understanding of the mechanics

This is an open access article under the terms of the [Creative Commons Attribution](https://creativecommons.org/licenses/by/4.0/) License, which permits use, distribution and reproduction in any medium, provided the original work is properly cited.

© 2025 The Author(s). *Engineering Reports* published by John Wiley & Sons Ltd.

of the system [7, 12–20]. For a detailed review of the literature surrounding transition zones, we refer the reader to works by Sañudo et al. [16], Indraratna et al. [21], and Fortunato et al. [22].

Experimental work has established methods for determining foundation properties [23–26] and investigating expected behaviours of the track at transition zones [9, 25, 27, 28], however, beyond this, investigations have largely been limited to numerical modeling [21] such as spectral Galerkin methods [29] and finite element methods, many of which are validated against empirical data. Finite element approaches have been particularly widely used, as they are effective at modeling the basic one dimensional case [10, 30], as well as more general two [31–33] and (most effectively) three [10–12, 27, 34–40] dimensional cases. Additionally, they can be more easily extended to non-linear theories, involving considerations of plastic deformations [34, 40, 41]. The most significant limitation of numerical methods is large computation times, which become particularly problematic when attempting to optimize track parameters. Recent research has worked to address this problem through the use of surrogate-assisted methods [30, 42, 43].

Although analytical solutions to some models do also exist [44–46], many are limited to finite beams [47–49], though others leverage a periodic track structure [33, 50–53]. In the absence of a transition zone, the steady-state deformation of the beam may easily be found using general solutions [44]. This is the basis for the approach taken by Sajjad et al. [7], who attempt to solve for the beam deformation around transition zones by superimposing solutions from multiple beams, each with a different uniform foundation stiffness. The recovered deformations are then used to inform the iterative design of multi-step transition zones. Whilst this approach is validated against numerical modeling for the cases considered in Reference [7], the solution obtained is only an approximate solution to the proposed model so it may not be valid under different conditions or changes to parameters. Also, it is important to note that the model only considers stationary loads. Dynamic amplification, which is considered to be important to the analysis of transition zones [19], is not directly present in this model. However, Sajjad et al. [7] multiply deformations by a dynamic amplification factor to account for this limitation.

The purposes of this paper are two-fold. The first is to respond to an absence in the literature of readily available, closed-form solutions for the steady-state deformation of an Euler-Bernoulli beam on a piece-wise homogeneous foundation with an arbitrary number of static point forces and foundation discontinuities (the model considered by Sajjad et al. [7], details of which are given in Section 2.1). Secondly, to apply the analytical solution to investigate the accuracy of the approximate solution proposed by Sajjad et al., which is summarized here in Section 2.2.

The derivation of the analytical solution is given in Section 2.3, wherein we divide the solution domain into homogeneous segments to which we can apply the method of undetermined coefficients. We then combine individual solutions by enforcing continuity conditions at the boundaries. Notably, this is similar to the method used in Reference [6] for a sinusoidal applied load in the context of subterranean tunnel design and the classical methods in Reference [5].

Enforcing the boundary conditions leads to a linear system of $4(n-1)$ variables for the coefficients of the general solution, where n is the number of beam segments (MATLAB code for constructing this matrix and solving for the deformation of the beam is provided in the Supporting Information). Recovering the solution to the system is then reduced to solving the linear system. Notably, for large systems, the matrices may be close to singular, and more advanced solution techniques may be required to improve accuracy. This is an avenue of further research and is not treated here.

A comparison between the approximate and analytical solutions is presented in Section 3. First, the effect of varying placement of point forces relative to transition zones is considered, specifically to highlight a limitation of the approximate solution. Following this, a comparison is also presented between the approximate and analytical solutions within the context of the graduated transition zones considered in Sajjad et al. [7]. Concluding statements are given in Section 4, followed by some remarks concerning the model itself in Section 5.

2 | Governing Equations and Solutions

2.1 | Governing Equations

The movement of an Euler-Bernoulli beam on a visco-elastic foundation with variable foundation stiffness is given by the partial differential equation

$$EI \frac{\partial^4 y}{\partial x^4} + m \frac{\partial^2 y}{\partial t^2} + C \frac{\partial y}{\partial t} + k(x)y = F(x) \quad (1)$$

where x (m) is the position along the axis of the beam, t (s) is time, y (m) is the vertical beam deformation, E (N/m²) is the Young's modulus of the beam, I (m⁴) is the moment of inertia of the beam, m (kg/m) is the mass per unit length of the beam, C (Ns/m²) is a damping coefficient, $k(x)$ (N/m²) is the stiffness of the foundation, and $F(x)$ (N/m) is an applied transverse load. Notably, this model ignores the effects of in-plane loads.

In this paper, we are concerned only with the static deformation of the beam. As such, Equation (1) reduces to an ordinary differential equation for the deformation of an infinite Euler-Bernoulli beam on an elastic foundation with variable stiffness:

$$EI \frac{d^4 y}{dx^4} + k(x)y = F(x) \quad (2)$$

To represent transition zones on the track, we model the beam stiffness as a step function of the form

$$k(x) = \begin{cases} k_0 & x \leq z_1, \\ k_1 & z_1 < x \leq z_2, \\ \vdots & \\ k_{\bar{n}-1} & z_{\bar{n}-1} < x \leq z_{\bar{n}}, \\ k_{\bar{n}} & z_{\bar{n}} < x \end{cases} \quad (3)$$

where k_i represent the stiffness of each beam segment, and z_i represent the locations of the transition zones. In this paper, we

TABLE 1 | Definition of variables used in this paper.

x	Position along the axis of the beam. (m)
y	Vertical deformation of the beam. (m)
y_a	Approximate vertical deformation. (m)
E	Young's modulus of Elasticity. (N/m ²)
I	Moment of Inertia. (m ⁴)
$k(x)$	Foundation stiffness. (N/m ²)
P	Strength of applied load. (N/m)
x_p	Position of applied load. (m)
n	Number of beam segments.
η	Number of boundaries.
L	Length of graduated transition zone. (m)
X_i	Starting position of i th gradation in graduated transition zone. (m)
Δk	Total change in foundation stiffness across the graduated transition zone. (N/m ²)

consider an applied load of the form

$$F(x) = \sum_{i=1}^m P_i \delta(x - x_{p,i}) \quad (4)$$

where P_i are the strengths of the point forces, $\delta(x)$ is the Dirac delta, and $x_{p,i}$ are the locations of the point forces for $i = 1, \dots, m$. However, since (2) is linear, we can solve for a single point force,

$$F(x) = P_i \delta(x - x_{p,i}) \quad (5)$$

and superimpose the solutions. For clarity, we describe the solution for a single point force of strength P at position x_p , which may be coincident with the transition zones z_i , giving rise to the governing equation

$$EI \frac{d^4 y}{dx^4} + k(x)y = P\delta(x - x_p) \quad (6)$$

We note that a summary of variables used in this paper is presented in Table 1.

2.2 | Approximate Solution

Previous work by Sajjad et al. [7] presents an “analytical approach” to determining the deformation of a beam in the model specified in Section 2.1. Their approach leverages superposition and existing general solutions of (6) to solve for the effect of each point force independently. Importantly, their solution is only an approximation to the model. Sajjad et al. [7] assume that the beam deformation depends only on the stiffness of the beam section on which the point force lies. They then solve for the beam deformation using a homogeneous foundation. A minor problem with this approach is that it is undefined for a point force that rests on a transition zone. A more significant problem is that the solution does not satisfy the governing equation in at least one (possibly

semi-infinite) section of the beam. The particular form of the solution used is written in Reference [7] as

$$w(x) = \sum_{p=1}^N \frac{P\beta_p}{2k} e^{-\beta(x-d_p)} [\cos(\beta(x-d_p)) + \sin(\beta(x-d_p))] \quad (7)$$

where N is the number of point forces, d_p is the location of the point force and is equivalent to the notation x_p used in this paper, w is the deformation of the beam and is equivalent to y , and $\beta = \sqrt[4]{k/EI}$.

Whilst (7) is the solution as written in Reference [7], it cannot be the correct form of the derived solution nor the form used for the calculations in Reference [7]. Firstly, it gives no indication of the changing stiffness. Secondly, in the development of the solution, Sajjad et al. [7] assume that the solution goes to zero in the limit as $|x| \rightarrow \infty$ and is symmetrical for a single point force. We suggest here the accurate form of Equation (7), namely

$$w(x) = \sum_{p=1}^N \frac{P\beta_p}{2k_p} e^{-\beta|x-d_p|} (\cos(\beta|x-d_p|) + \sin(\beta|x-d_p|)) \quad (8)$$

where k_p is the beam stiffness associated with the point force at x_p , and $\beta_p = \sqrt[4]{k_p/EI}$. This form satisfies the boundary and symmetry conditions that (7) does not and produces results that are at least qualitatively indistinguishable from those produced and verified by Sajjad et al. [7].

2.3 | Analytical Solution

To solve Equation (6), we make the observation that it is a linear and piece-wise constant coefficient. Hence, by dividing the domain into (possibly semi-infinite) segments, whose boundaries are prescribed by the coordinates of the transition zones and point force, we can reduce the problem to an ordinary differential equation with constant coefficients. Then, we can apply the method of undetermined coefficients and create a full solution by enforcing continuity conditions at the boundaries between each segment.

By enforcing zero deformation in the limit as x goes to $\pm\infty$, the general solution to (6) (see Appendix A) is given by

$$y(x) = \begin{cases} c_1 e^{\sqrt[4]{k_0/EI} m_1 x} + c_2 e^{\sqrt[4]{k_0/EI} m_2 x} & x < x_1, \\ \sum_{j=1}^4 c_{j+2} e^{\sqrt[4]{k_1/EI} m_j x} & x_1 < x < x_2, \\ \vdots & \\ \sum_{j=1}^4 c_{\eta-4+j} e^{\sqrt[4]{k_{\eta-1}/EI} m_j x} & x_{\eta-1} < x < x_\eta, \\ c_{4\eta-1} e^{\sqrt[4]{k_\eta/EI} m_3 x} + c_{4\eta} e^{\sqrt[4]{k_\eta/EI} m_4 x} & x_\eta < x \end{cases} \quad (9)$$

where $x_i, i = 1, \dots, \eta$, are the locations of the boundaries between segments, k_i are the stiffnesses in these segments, $c_j, j = 1, \dots, 4m$, are complex valued coefficients, and where $i = \sqrt{-1}$. Clearly, there are two possibilities for the number of boundaries, η . Either η is one greater than the number of transition zones (the positions of the transition zones and point force, z_i and x_p , are

distinct for all i) or η is equal to the number of transition zones ($z_i = x_p$ for some i , in which case the point force sits directly on a transition zone).

From this, it remains to solve for the coefficients c_j , which is simply done by implementing boundary conditions at positions x_i and forming a system of linear equations. At transition zones that do not coincide with a point force, we enforce the continuity of the solution and its first three derivatives. At a point force (on a transition zone or otherwise) we enforce the continuity of the function and its first two derivatives. Continuity of the function at a point force implies a discontinuity of the third derivative proportional to the strength of the point force (see Appendix B). The equations arising from implementing these conditions can be found in Appendix C.

Implementing these boundary conditions gives a matrix equation of the form $\mathbf{A}\mathbf{c} = \mathbf{b}$. The column vector \mathbf{b} is a vector of zeroes except at b_{4i} if x_i is the location of the point force, in which case $b_{4i} = P/EI$. For example, if the system is composed of a point force of strength P at x_1 and a transition zone stepping from k_1 to k_2 at x_2 , then, in such case, the column vector \mathbf{b} would be found to be

$$\mathbf{b} = \begin{bmatrix} 0 \\ 0 \\ 0 \\ P/EI \\ 0 \\ 0 \\ 0 \\ 0 \end{bmatrix} \quad (10)$$

The column vector $\mathbf{c} = (c_1, \dots, c_{4\eta})^T$, is formed directly from the unknown coefficients, and \mathbf{A} is a matrix of the form

$$\mathbf{A} = \begin{bmatrix} \mathbf{A}_1 & -\mathbf{B}_1 & \mathbf{0} & \mathbf{0} & \mathbf{0} & \dots & \mathbf{0} \\ \mathbf{0} & \mathbf{A}_2 & -\mathbf{B}_2 & \mathbf{0} & \mathbf{0} & \dots & \mathbf{0} \\ \vdots & \ddots & \ddots & \ddots & \ddots & & \vdots \\ \mathbf{0} & \dots & \mathbf{0} & \mathbf{A}_{\eta-1} & -\mathbf{B}_{\eta-1} & \mathbf{0} \\ \mathbf{0} & \dots & \mathbf{0} & \mathbf{A}_{\eta} & -\mathbf{B}_{\eta} \end{bmatrix} \quad (11)$$

where the $\mathbf{0}$ are zero-valued submatrices of appropriate size, and $\mathbf{A}_1 \in M_{4 \times 2}$ and $\mathbf{A}_i \in M_{4 \times 4}$, $i = 2, \dots, \eta$ are submatrices given by

$$\mathbf{A}_1 = \left[a_{j,\tilde{z}}^1 \right]_{j=3,\tilde{z}=0}^{4,3}, \quad (12a)$$

$$\mathbf{A}_i = \left[a_{j,\tilde{z}}^i \right]_{j=1,\tilde{z}=0}^{4,3}, \quad (12b)$$

$$a_{j,\tilde{z}}^i = \left(\sqrt[4]{k_{i-1}/EI} m_j \right)^{\tilde{z}} e^{\sqrt[4]{k_{i-1}/EI} x_i} \quad (12c)$$

Similarly, $\mathbf{B}_{\eta} \in M_{4 \times 2}$ and $\mathbf{B}_i \in M_{4 \times 4}$, $i = 1, \dots, \eta - 1$ are complex-valued matrices given by

$$\mathbf{B}_i = \left[b_{j,\tilde{z}}^i \right]_{j=1,\tilde{z}=0}^{4,3}, \quad (13a)$$

$$\mathbf{B}_{\eta} = \left[b_{j,\tilde{z}}^{\eta} \right]_{j=1,\tilde{z}=0}^{2,3}, \quad (13b)$$

$$b_{j,\tilde{z}}^i = \left(\sqrt[4]{k_i/EI} m_j \right)^{\tilde{z}} e^{\sqrt[4]{k_i/EI} x_i} \quad (13c)$$

Figure 1 shows the general structure of the matrix \mathbf{A} for five boundaries, that is, $\eta = 5$.

We note that the construction of the matrix \mathbf{A} and the right-hand-side vector \mathbf{b} within a computer program is not a trivial process. This is especially true if the goal is to be able to quickly input an arbitrary set of transition zones and point forces. The provided MATLAB code, in the Supporting Information, includes a purpose-built class that contains all the methods we expect to be commonly required.

It is also worth noting that each additional boundary (i.e., point force, transition zone, or coinciding transition zone and point force) adds four rows and columns to matrix \mathbf{A} . In this way, solving for each point force and then superimposing serves to limit the size of the matrices that need to be inverted. The described method may be easily extended to calculate the displacement for all point forces simultaneously, if that is desired, or for abrupt changes in beam stiffness EI . These cases, however, are not dealt with in this paper nor are they implemented in the MATLAB code in the Supporting Information.

3 | Comparison Between Analytical and Approximate Solutions

In this section, we compare the beam deformations as predicted by the approximate solution to those of the closed-form solution. This is with the goal of providing insight into the behavior of the approximate solution.

The broad behavior of the approximate solution was presented in Reference [7] and validated against numerical models for the relevant use cases. Here we consider cases chosen to display situations in which the approximate solution may not approximate the model. Specifically, we look at the case of a single point force placed close to a transition zone (Section 3.1), and the behavior of the approximate solution as the number of gradations is increased for a graduated transition zone as in Equation (14) (Section 3.2). Notably, throughout this section, we choose to report the absolute errors or strict differences between the analytic and approximate deformations $|y - y_a|$ in preference over relative errors. This is done to give a sense of the scale of the errors to the dimensions of the track infrastructure.

The parameters used for the analysis in this section are chosen to correspond to those for which the approximate method was validated in Reference [7]. The Young's modulus of the beam is

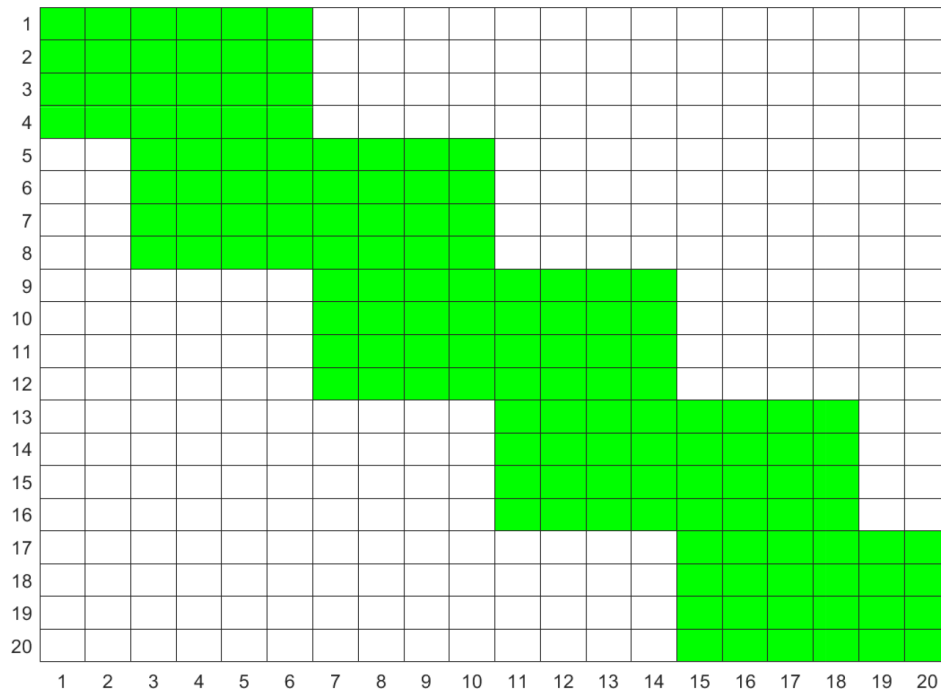


FIGURE 1 | Example of structure of matrix A for five boundaries. Non-zero elements are marked in green, and zero elements are marked in white.

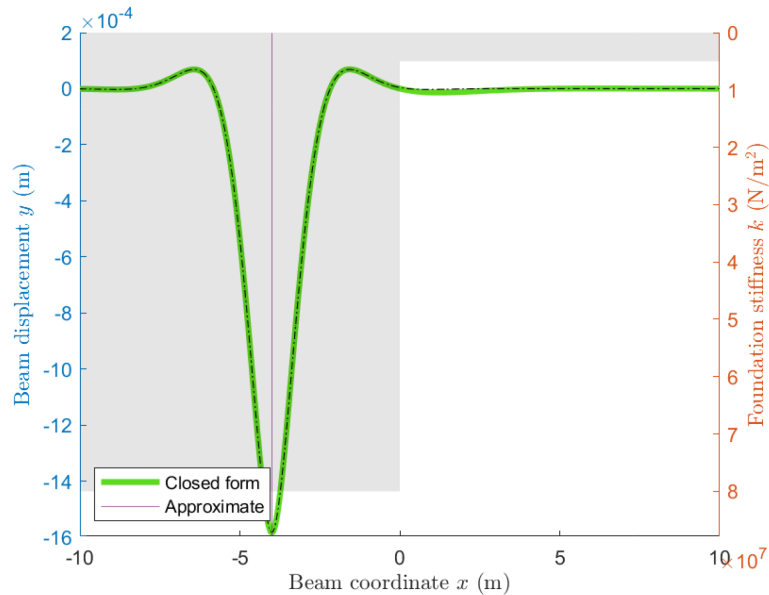


FIGURE 2 | Point force applied away from transition zone, at $x = -4$, gives good match between closed-form and approximate solution.

given as $E = 2.1 \times 10^{11} \text{ N/m}^2$, the moment of inertia can be calculated from the geometry of the beam cross-section as $I = 3.42 \times 10^{-5} \text{ m}^4$, chosen to correspond to UIC60 rail [7], and the strength of the applied load can be calculated to be $P = -9.8 \times 10^4 \text{ N/m}$ which corresponds to a 10 t load. The values of the foundation stiffness k vary throughout the section and are given as used.

3.1 | One Transition Zone

In the absence of transition zones, the approximate solution developed in Reference [7] gives results that are algebraically

equivalent to the method described in this paper, as a consequence of both methods being an implementation of preexisting general solutions. The results begin to differ, however, as transition zones are introduced. In this section, we analyze the discrepancy between the closed-form solution and approximate solution for varying placements of a point force and with a transition zone at $x = 0$, over which the foundation stiffness changes from $80 \times 10^6 \text{ N/m}^2$ to $5 \times 10^6 \text{ N/m}^2$.

Figure 2 shows the closed-form solution plotted against the approximate solution for a point forced placed 4 meters from the transition zone. The two approaches match well over the entire

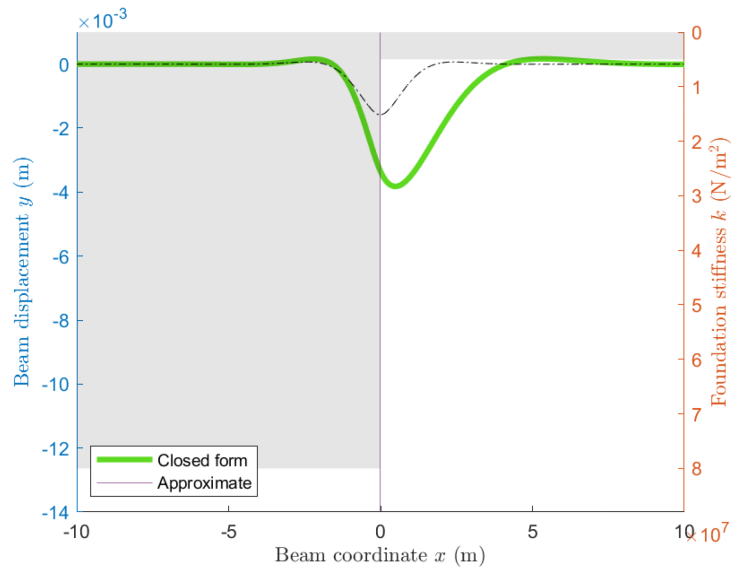


FIGURE 3 | Closed-form vs. approximate solution for a single transition zone at $x = 0$ and a point force at $x = -0.1$ (shown with vertical line).

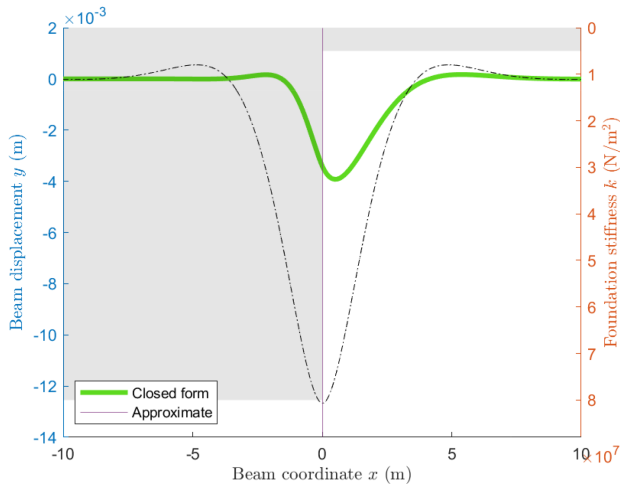


FIGURE 4 | Closed-form vs. approximate solution for a single transition zone at $x = 0$ and a point force at $x = 0.1$ (shown with vertical line).

plot, differing most significantly near the transition zone. Given that the approximate solution only uses the stiffness where the point force is applied, and hence does not consider the transition zone, this behavior is expected.

Following this argument, it is expected that the two solutions will differ most significantly when the point force is close to the transition zone. Furthermore, a small change in the placement of the point force across a transition zone should cause only a small change in the displacement of the closed-form solution but will result in abrupt and significant changes in the approximate solution. This phenomenon is demonstrated in Figures 3 and 4, where significant differences between the two approaches are readily observed (approximately 1–6 mm). To the left of the transition zone, the maximum deformation is significantly underestimated by the approximate solution as it fails to take into account the nearby region of low stiffness and conversely to the right of the transition zone. This is illustrated more

precisely in Figure 5, which shows the most extreme value of the difference between the analytical solution and approximate solution, $y - y_a$, for various values of the position of the point force x_p and with a transition zone at $x = 0$. As previously mentioned, away from the transition zone, the difference between the two approaches is negligible. The difference gradually increases closer to the transition zone before abruptly changing as the point force moves from being applied on the stiffer beam segment to the less rigid segment. Around the transition zone, the error reaches a high of approximately 5mm, close to 2.5 times the predicted deformation from the analytical solution. There are also smaller abrupt changes present at $x \approx -1$ and 3 which are associated with a change in sign when the most extreme value changes between being associated with an under-approximation (over-approximation) at the transition zone and being associated with an over-approximation (under-approximation) at the point force. Another observation we can make here is that, for the approximate solution, the maximum deformation occurs precisely at the point force. For the analytical solution however, the maximum deformation is offset, which aligns more closely to the behavior of 3D finite element models, as can be seen in Reference [35].

3.2 | Graduated Transition Zone

Using the same distribution of point forces as in Reference [7] (see Table 2) we investigate the behavior of the approximate and closed-form solutions for graduated transition zones. As proposed in Reference [7], graduated transition zones replace a single transition zone with multiple, equal-length segments (referred to in this paper as “gradations”) of decreasing stiffness. The stiffness of these sections is given by the formula

$$k_i = \Delta k \times e^{(7 \times 10^{-4} L - 0.1) X_i} + k_{n+1} \quad (14)$$

where k_i , $i = 0, \dots, n$, is the stiffness to the left of the i th transition zone, k_{n+1} is the stiffness to the right of the graduated transition zone, $\Delta k = k_{n+1} - k_0$ is the total stiffness change across

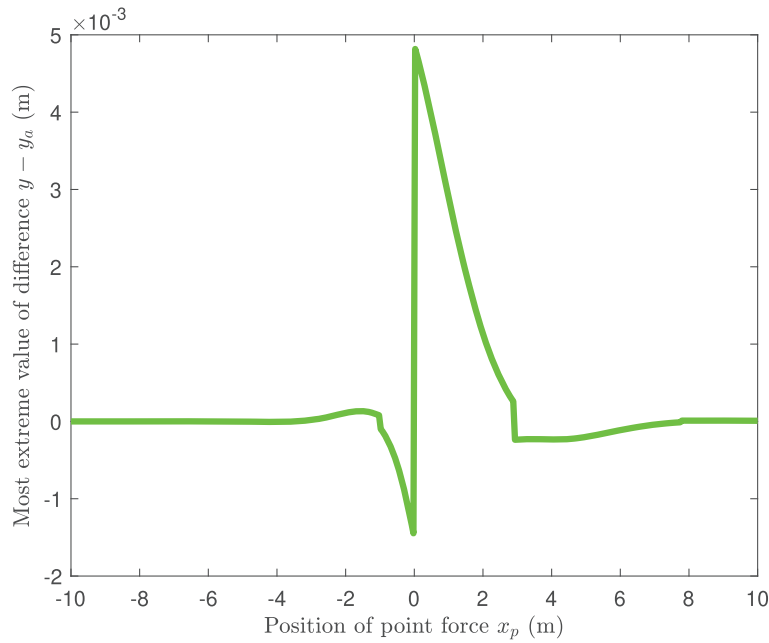


FIGURE 5 | Most extreme difference in deformation between closed-form and approximate solution plotted against the position of a single point force with a transition zone at $x = 0$.

TABLE 2 | Positions of point forces as used in [7] and investigated in Section 3.2.

x_1	x_2	x_3	x_4	x_5	x_6	x_7	x_8
-29.75	-27.25	-15.25	-12.75	-8.75	-6.25	5.75	8.25
x_9	x_{10}	x_{11}	x_{12}	x_{13}	x_{14}	x_{15}	x_{16}
12.25	14.75	26.75	29.25	33.25	35.75	47.75	50.25

the graduated transition zone, L is the length of the graduated transition zone, and X_i is the location of the i th transition zone. In particular, we take $L = 40$ m, $k_0 = 80 \times 10^6$ N/m², $k_n = 5 \times 10^6$ N/m², and space all transition zone locations, X_i , evenly between $x = 0$ and $x = L$. We do, however, make one notable exception in our analysis. The formula for k_i , as written, leaves a significant gap between the stiffness k_n and k_{n+1} that does not smooth out as the number of transition zones increases. We believe that this is an unintended effect and since it overshadows errors associated with the graduated transition zones, we choose to modify the formula, even if it is at a minor loss in accordance with the physical context. To this end, we set the furthest right stiffness to

$$\Delta k \times e^{(7 \times 10^{-4} L - 0.1)(n+1)L/n} + k_{n+1} \quad (15)$$

rather than k_{n+1} .

Figures 6–8 show the deformation of the beam as the number of gradations in the graduated transition zone is increased. Notably, we see similar behavior as occurred with a single point force and transition zone. That is, the most significant differences occur at the transition zones, especially when a point force is close to the transition zone. A markedly higher deformation at approximately $x = 50$ m is related only to the closer proximity of the point forces at x_{15} and x_{16} , as compared with the other point forces.

Comparing Figures 6 and 8, the agreement between the two approaches appears to improve as the number of transition zones increases. At certain points, however, the difference may increase significantly, as illustrated by Figure 7, specifically at $x \approx 12$ and 27. Figure 9, which graphs the most extreme absolute difference between the closed-form and approximate solutions for an increasing number of transition zones, shows this trend for the system described here. As the number of additional transition zones (i.e., gradations) is increased, the absolute difference between the analytical and approximate solutions is unstable, but generally decreases. After adding approximately 25 transition zones, the instability is no longer observable, and the difference begins to converge to and oscillate around, approximately 0.2×10^{-4} m. The early erratic behavior of this graph can be attributed to the proximity of transition zones and point forces. Due to the process by which transition zones are added, the positions of all but the first transition zone change. As such, the difference between the two approaches may increase sharply if a transition zone moves close to or is added near a point force. This effect is most notable when there are few transition zones, and relative positions change by larger amounts to fit evenly within the space. On the other hand, the gradual decrease in error is associated with the gradual decrease in the difference in stiffness across each transition zone. As the change in stiffness becomes spread over a larger area, so too do the errors associated with the approximate solution. This reduction holds only to a point, however. More

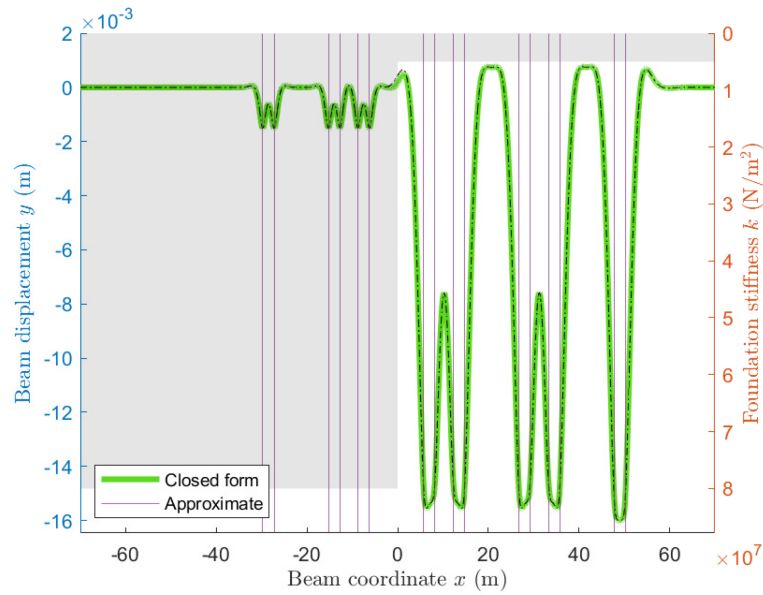


FIGURE 6 | Deformation of a beam with a single transition zone under the effect of multiple point forces (shown as vertical lines) as listed in Table 2.

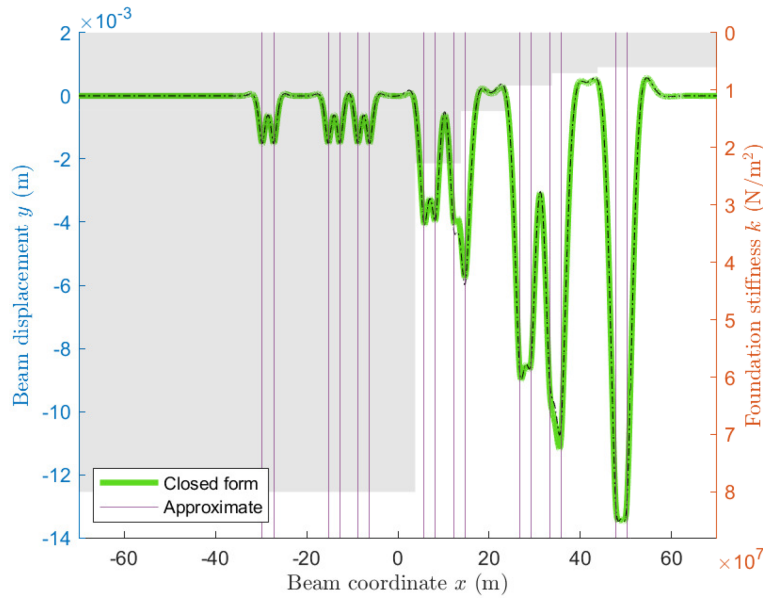


FIGURE 7 | Deformation of a beam with a graduated transition zone with 4 gradations under the effect of multiple point forces (shown as vertical lines) as listed in Table 2.

research is necessary before a conclusion can be made, although it would appear that, in the limiting case, the analytical solution approaches the correct value for a smooth transition (as opposed to piece-wise), while the approximate solution does not.

The approximate threshold value of 25 transition zones and limiting error of 0.2×10^{-4} m are dependent on the parameters of the model and hence cannot be used as rules. While specific results relating to convergence properties are beyond the scope of this paper, some general comments can still be made. The broad properties displayed in Figure 9 and discussed above hold for small changes to the position of the point forces and significant changes to the magnitudes of the parameters E and I with

deformation magnitudes scaling at approximately the order of the fourth derivative of the parameters in this latter case. For the axle load P , the deformations and errors both scale directly—that is, a doubling of the axle load will result in a doubling of all deformations. Rigorous analysis of the convergence properties of the approximate solution to the closed-form solution under varying conditions is an avenue for future study.

4 | Conclusion

Abrupt changes in foundation stiffness underneath rail track can create differential plastic settlements, which increase dynamic

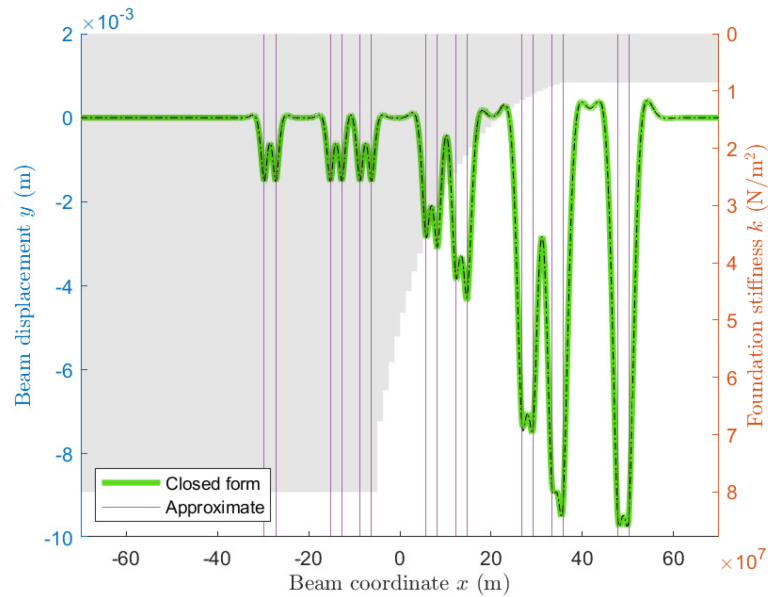


FIGURE 8 | Deformation of a beam with a graduated transition zone with 32 gradations under the effect of multiple point forces (shown as vertical lines) as listed in Table 2.

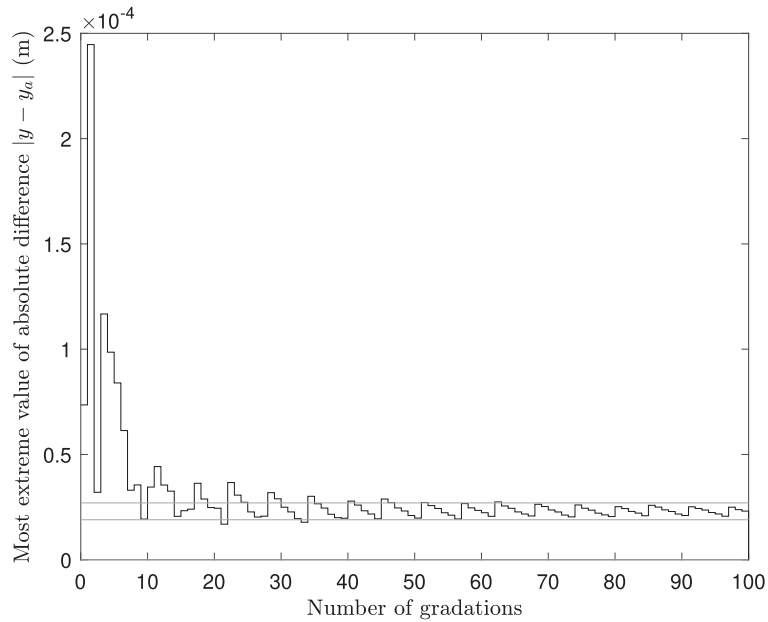


FIGURE 9 | Most extreme absolute difference between the closed-form and approximate solutions for an increasing number of transition zones, parameters as specified in Section 3.2. With sufficiently many transition zones, the difference is between approximately 0.19×10^{-4} m and 0.27×10^{-4} m, indicated by the two red lines.

loads, track deterioration, and passenger discomfort, thereby necessitating more frequent maintenance [7, 12]. This motivates research into the deformation of rail tracks around these transition zones. Responding to an absence in the literature of readily available closed-form solutions for the steady-state deformation of an Euler-Bernoulli beam on a visco-elastic foundation, with multiple abrupt changes in stiffness and point forces, we developed such a solution. The deformation is found in terms of the solution of a linear system by splitting the beam into homogeneous segments and enforcing continuity conditions at the

boundary. Using this solution, we carried out an analysis of a previously published technique [7], and drew particular attention to situations in which it may have larger errors. Specifically, this was found to be when point forces are close to transition zones and is highest when a point force is placed on the less stiff side of the transition zone where the error was observed to reach a high of approximately 5 mm, close to 2.5 times the predicted deformation from the analytical solution. The error in the approximate solution was also assessed as it related to the use of the graduated transition zones for which it was used in the original

publication [7]. For low numbers of intermediary transition zones (i.e., approximately 0–10), the errors fluctuate but stayed below 2.5×10^{-4} m, before decaying in an oscillatory manner to less than 0.27×10^{-4} m.

Ultimately, the approximation technique presented by [7] is an effective method for rapidly estimating the beam deformation, but may not adequately approximate the model under certain conditions and should be applied with careful consideration. The closed-form solution improves the solution method used by Sajjad et al. [7] in that it provides more accurate results to the model studied in this paper.

5 | Remarks on Current Model

Mathematically, the closed-form solution presented in this paper is derived based on analysis of stresses and motion equations coupled with elastic behavior. Even though it provides a more accurate solution in attempts to model railway tracks and transition zones compared to [7], there are limitations of the model (i.e., Euler-Bernoulli beam theory) in capturing the properties at the transition zones. The Euler-Bernoulli beam equation with visco-elastic foundation, and the related static equation, are dependent on elastic theories whereas the constitutive behavior of materials in transition zones is not. As the settlement in transition zones is elasto-plastic and dependent on the behavior of materials used to fill the zones, the deformation may be irrecoverable under the heavy axle loads of freight trains. The analysis in this paper complies only with small-strain and small-displacement theories, while, in reality, the deformations conform more accurately to large-strain and large-displacements theories. The treatment of more accurate elasto-plastic models for analytical progress is a subject of future research. Nevertheless, we refer the reader to recent work in this space using finite element methods such as [27, 32], and also to [21], which presents a review of research into the modeling and improvement of transition zones.

Author Contributions

Josiah Murray: investigation; conceptualization; writing – original draft; writing – review and editing; visualization; validation; methodology; software; formal analysis; data curation. **Michael H. Meylan:** conceptualization; investigation; methodology; formal analysis; supervision; software; validation; visualization. **Trung Ngo:** conceptualization; writing – original draft; data curation; resources; software; methodology; validation; funding acquisition; visualization. **Ngamta Thamwattana:** conceptualization; writing – original draft; writing – review and editing; funding acquisition; visualization; project administration; supervision; resources; formal analysis. **Buddhima Indraratna:** writing – original draft; resources; project administration; funding acquisition; conceptualization; validation; methodology; visualization.

Acknowledgments

The authors are grateful to the Australian Research Council for the funding of Discovery Project DP220102862.

Conflicts of Interest

The authors declare no conflicts of interest.

Data Availability Statement

The data that supports the findings of this study are available in the Supporting Information of this article.

References

1. B. Indraratna, P. Baral, Y. Qi, T. Ngo, C. Rujikiatkamjorn, and F. Ferreira, “Advances in Ground Improvement and Principles of Track Geomechanics for Future Railways,” in *Proceedings of the 17th African Regional Conference on Soil Mechanics and Geotechnical Engineering*, (2020), 1–16.
2. BITRE, “Trainline 10,” Canberra, May, 2023.
3. B. Indraratna, Q. Sun, N. T. Ngo, and C. Rujikiatkamjorn, “Current Research Into Ballasted Rail Tracks: Model Tests and Their Practical Implications,” *Australian Journal of Structural Engineering* 18, no. 3 (2017): 204–220, <https://doi.org/10.1080/13287982.2017.1359398>.
4. B. Indraratna, Y. Qi, R. S. Malisetty, S. K. Navaratnarajah, F. Mehmood, and M. Tawk, “Recycled Materials in Railroad Substructure: An Energy Perspective,” *Railway Engineering Science* 30, no. 3 (2022): 304–322, <https://doi.org/10.1007/s40534-021-00267-6>.
5. M. Hetenyi, *Beams on Elastic Foundation: Theory With Applications in the Fields of Civil and Mechanical Engineering*, vol. 1, 4th ed., ed. G. Cumberlege (Oxford University Press, 1955), 1–255.
6. H. Yu, Z. Zhang, J. Chen, A. Bobet, M. Zhao, and Y. Yuan, “Analytical Solution for Longitudinal Seismic Response of Tunnel Liners With Sharp Stiffness Transition,” *Tunnelling and Underground Space Technology* 77 (2018): 103–114, <https://doi.org/10.1016/j.tust.2018.04.001>.
7. M. B. Sajjad, B. Indraratna, T. Ngo, R. Kelly, and C. Rujikiatkamjorn, “A Computational Approach to Smoothen the Abrupt Stiffness Variation Along Railway Transitions,” *Journal of Geotechnical and Geoenvironmental Engineering* 149, no. 8 (2023): 04023063, <https://doi.org/10.1061/JGGEFK.GTENG>, <https://orcid.org/0000-0002-9676-3728>.
8. S. Narendar, S. S. Gupta, and S. Gopalakrishnan, “Wave Propagation in Single-Walled Carbon Nanotube Under Longitudinal Magnetic Field Using Nonlocal Euler–Bernoulli Beam Theory,” *Applied Mathematical Modelling* 36, no. 9 (2012): 4529–4538 0307904X, <https://doi.org/10.1016/j.apm.2011.11.073>.
9. C. Qu, X. Tan, Y. Xiao, Z. Wang, and L. Wei, “Subgrade Vibrations and Long-Term Stability of an Embankment-Bridge Transition Zone in Non-Ballasted High-Speed Railway,” *Transportation Geotechnics* 45 (2024): 101199, <https://doi.org/10.1016/j.trgeo.2024.101199>.
10. J. N. Varandas, P. Hölscher, and M. A. G. Silva, “Dynamic Behaviour of Railway Tracks on Transitions Zones,” *Computers & Structures* 89, no. 13–14 (2011): 1468–1479, <https://doi.org/10.1016/j.compstruc.2011.02.013>.
11. Z. Jabbar-Ali and V. Ghorbani, “Investigation on Dynamic Behavior of Railway Track in Transition Zone,” *Journal of Mechanical Science and Technology* 25, no. 2 (2011): 287–292, <https://doi.org/10.1007/s12206-010-1202-x>.
12. M. Labrado Palomo, F. Roca Barceló, F. Ribes Llarío, and J. Real Heráiz, “Effect of Vehicle Speed on the Dynamics of Track Transitions,” *Journal of Vibration and Control* 24, no. 21 (2017): 107754631774525, <https://doi.org/10.1177/1077546317745254>.
13. T. Xin, Y. Ding, P. Wang, and L. Gao, “Application of Rubber Mats in Transition Zone Between Two Different Slab Tracks in High-Speed Railway,” *Construction and Building Materials* 243 (2020): 118219, <https://doi.org/10.1016/j.conbuildmat.2020.118219>.
14. A. Jain, A. V. Metrikine, M. J. M. M. Steenbergen, and K. N. van Dalen, “Railway Transition Zones: Evaluation of Existing Transition Structures and a Newly Proposed Transition Structure,” *International Journal of Rail Transportation* 12, no. 6 (2024): 979–999, <https://doi.org/10.1080/23248378.2023.2272668>.

15. A. Ramos, R. Calçada, and A. G. Correia, "Influence of Train Speed and Its Mitigation Measures in the Short- and Long-Term Performance of a Ballastless Transition Zone," *Railway Engineering Science* 31, no. 4 (2023): 309–324, <https://doi.org/10.1007/s40534-023-00314-4>.
16. R. Sa nudo, L. dell'Olio, J. A. Casado, I. A. Carrascal, and S. Diego, "Track Transitions in Railways: A Review," *Construction and Building Materials* 112 (2016): 140–157, <https://doi.org/10.1016/j.conbuildmat.2016.02.084>.
17. R. Sa nudo, I. Jardí, J.-C. Martínez, et al., "Monitoring Track Transition Zones in Railways," *Sensors* 22, no. 1 (2021): 76, <https://doi.org/10.3390/s22010076>.
18. A. Jain, A. V. Metrikine, M. J. M. M. Steenbergen, and K. N. van Dalen, "Design of Railway Transition Zones: A Novel Energy-Based Criterion," *Transportation Geotechnics* 46 (2024): 101223, <https://doi.org/10.1016/j.trgeo.2024.101223>.
19. A. Jain, K. N. van Dalen, M. J. M. M. Steenbergen, and A. V. Metrikine, "Dynamic Amplifications in Railway Transition Zones: Investigation of Key Phenomena," *Journal of Physics: Conference Series* 2647, no. 15 (2024): 152002, <https://doi.org/10.1088/1742-6596/2647/15/152002>.
20. B. Indraratna, S. Nimbalkar, and S. K. Navaratnarajah, "Use of Shock Mats for Mitigating Degradation of Railroad Ballast," *Sri Lankan Geotechnical Journal - Special Issue on Ground Improvement* 6, no. 1 (2014): 32–41.
21. B. Indraratna, M. B. Sajjad, T. Ngo, A. G. Correia, and R. Kelly, "Improved Performance of Ballasted Tracks at Transition Zones: A Review of Experimental and Modelling Approaches," *Transportation Geotechnics* 21 (2019): 100260, <https://doi.org/10.1016/j.trgeo.2019.100260>.
22. E. Fortunato, A. Paixao, and R. Calçada, "Railway Track Transition Zones: Design, Construction, Monitoring and Numerical Modelling," *International Journal of Railway Technology* 2, no. 4 (2013): 33–58, <https://doi.org/10.4203/ijrt.2.4.3>.
23. F. Lamas-Lopez, Y.-J. Cui, N. Calon, S. Costa D'Aguiar, and T. Zhang, "Impact of Train Speed on the Mechanical Behaviours of Track-Bed Materials," *Journal of Rock Mechanics and Geotechnical Engineering* 9, no. 5 (2017): 818–829, <https://doi.org/10.1016/j.jrmge.2017.03.018>.
24. T. W. Zhang, F. Lamas-Lopez, Y.-J. Cui, N. Calon, and S. Costa D'Aguiar, "Development of a Simple 2D Model for Railway Track-Bed Mechanical Behaviour Based on Field Data," *Soil Dynamics and Earthquake Engineering* 99 (2017): 203–212, <https://doi.org/10.1016/j.soildyn.2017.05.005>.
25. T. W. Zhang, Y. J. Cui, F. Lamas-Lopez, N. Calon, and S. Costa D'Aguiar, "Modelling Stress Distribution in Substructure of French Conventional Railway Tracks," *Construction and Building Materials* 116 (2016): 326–334, <https://doi.org/10.1016/j.conbuildmat.2016.04.137>.
26. Z. Cai, G. P. Raymond, and R. J. Bathurst, "Estimate of Static Track Modulus Using Elastic Foundation Models," *Transportation Research Record* 1470 (1994): 65.
27. G. Jing, M. Siahkouhi, H. Wang, and M. Esmaeili, "The Improvement of the Dynamic Behavior of Railway Bridge Transition Zone Using Furnace Slag Reinforcement: A Numerical and Experimental Study," *Proceedings of the Institution of Mechanical Engineers, Part F: Journal of Rail and Rapid Transit* 236, no. 4 (2022): 362–374, <https://doi.org/10.1177/09544097211020603>.
28. F. Lamas-Lopez, Y.-J. Cui, N. Calon, S. Costa D'Aguiar, M. De Peixoto Oliveira, and T. Zhang, "Track-Bed Mechanical Behaviour Under the Impact of Train at Different Speeds," *Soils and Foundations* 56, no. 4 (2016): 627–639, <https://doi.org/10.1016/j.sandf.2016.07.004>.
29. R. T. R. Walker and B. Indraratna, "Moving Loads on a Viscoelastic Foundation With Special Reference to Railway Transition Zones," *International Journal of Geomechanics* 18, no. 11 (2018): 04018145, [https://doi.org/10.1061/\(ASCE\)GM.1943-5622.0001274](https://doi.org/10.1061/(ASCE)GM.1943-5622.0001274).
30. Y. Shang, M. Nogal, R. Teixeira, and A. R. R. M. Wolfert, "Optimal Design of Rail Level Crossings and Associated Transition Zones Using Adaptive Surrogate-Assisted Optimization," *Engineering Structures* 282 (2023): 115740, <https://doi.org/10.1016/j.engstruct.2023.115740>.
31. K. Nasrollahi, J. C. Nielsen, E. Aggestam, J. Dijkstra, and M. Ekh, "Prediction of Differential Track Settlement in Transition Zones Using a Non-Linear Track Model," in *Advances in Dynamics of Vehicles on Roads and Tracks II*, 1st ed., ed. A. Orlova and D. Cole (Springer Cham, 2022), 282–292, https://doi.org/10.1007/978-3-031-07305-2_29.
32. K. Nasrollahi, J. C. O. Nielsen, E. Aggestam, J. Dijkstra, and M. Ekh, "Prediction of Long-Term Differential Track Settlement in a Transition Zone Using an Iterative Approach," *Engineering Structures* 283 (2023): 115830, <https://doi.org/10.1016/j.engstruct.2023.115830>.
33. X. Zhang, D. Thompson, and X. Sheng, "Differences Between Euler-Bernoulli and Timoshenko Beam Formulations for Calculating the Effects of Moving Loads on a Periodically Supported Beam," *Journal of Sound and Vibration* 481 (2020): 115432, <https://doi.org/10.1016/j.jsv.2020.115432>.
34. J. Bronsert, M. Baeßler, P. Cuéllar, and W. Rücker, "Numerical Modeling of Train-Track-Interaction at Bridge Transition Zones Considering the Long-Term Behaviour," in *Proceedings of the 11th International Conference on Vibration Problems*, ed. Z. Dimitrovova and A. Bracciali (AMP-TAC, 2013).
35. A. Jain, A. V. Metrikine, and K. N. van Dalen, "Energy Redistribution in Railway Transition Zones by Geometric Optimisation of a Novel Transition Structure," *Transportation Geotechnics* 49 (2024): 101383, <https://doi.org/10.1016/j.trgeo.2024.101383>.
36. H. Heydari-Noghabi, J. N. Varandas, J. A. Zakeri, and M. Esmaeili, "Performance Evaluation of a Combined Transition System in Slab-Ballasted Railway Track Using a Vehicle-Track-Substructure Interaction Model," *KSCE Journal of Civil Engineering* 27, no. 9 (2023): 3848–3860, <https://doi.org/10.1007/s12205-023-1273-8>.
37. Q. Sun, B. Indraratna, and J. Grant, "Numerical Simulation of the Dynamic Response of Ballasted Track Overlying a Tire-Reinforced Capping Layer," *Frontiers in Built Environment* 6 (2020): 2297–3362, <https://doi.org/10.3389/fbuil.2020.00006>.
38. A. Paixão, J. N. Varandas, E. Fortunato, and R. Calçada, "Numerical Simulations to Improve the Use of Under Sleeper Pads at Transition Zones to Railway Bridges," *Engineering Structures* 164 (2018): 169–182, <https://doi.org/10.1016/j.engstruct.2018.03.005>.
39. A. Paixao, J. N. Varandas, and E. Fortunato, "Dynamic Behavior in Transition Zones and Long-Term Railway Track Performance," *Frontiers in Built Environment* 7 (2021): 2297–3362, <https://doi.org/10.3389/fbuil.2021.658909>.
40. A. Tucho, B. Indraratna, and T. Ngo, "Stress-Deformation Analysis of Rail Substructure Under Moving Wheel Load," *Transportation Geotechnics* 36 (2022): 100805, <https://doi.org/10.1016/j.trgeo.2022.100805>.
41. S. Yao, Y. Shan, S. Zhou, B. Wang, and C. L. Ho, "Differential Settlement Prediction of Ballasted Tracks in Bridge–Embankment Transition Zones," *Journal of Geotechnical and Geoenvironmental Engineering* 146, no. 9 (2020): 04020075, [https://doi.org/10.1061/\(ASCE\)GT.1943-5606.0002307](https://doi.org/10.1061/(ASCE)GT.1943-5606.0002307).
42. A. Jain, Y. Marykovskiy, A. V. Metrikine, and K. N. van Dalen, "Quantifying the Impact of Stiffness Distributions on the Dynamic Behaviour of Railway Transition Zones," *Transportation Geotechnics* 45 (2024): 101211, <https://doi.org/10.1016/j.trgeo.2024.101211>.
43. A. Ramos, A. Castanheira-Pinto, A. Colaço, J. Fernández-Ruiz, and P. Alves Costa, "Predicting Critical Speed of Railway Tracks Using Artificial Intelligence Algorithms," *Vibration* 6, no. 4 (2023): 895–916, <https://doi.org/10.3390/vibration6040053>.
44. L. Fryba, *Vibrations of Solids and Structures Under Moving Loads* (Noordhoff International Publishing, 1972), 9001324202.

45. Z. Cai, G. P. Raymond, and R. J. Bathurst, "Natural Vibration Analysis of Rail Track as a System of Elastically Coupled Beam Structures on Winkler Foundation," *Computers & Structures* 53, no. 6 (1994): 1427–1436, [https://doi.org/10.1016/0045-7949\(94\)90408-1](https://doi.org/10.1016/0045-7949(94)90408-1).
46. P. Koziol and D. Kudla, "Vertical Vibrations of Rail Track Generated by Random Irregularities of Rail Head Rolling Surface," *Journal of Physics: Conference Series* 1106 (2018): 012007, <https://doi.org/10.1088/1742-6596/1106/1/012007>.
47. D. Adair, A. Ibrayev, J. R. Kim, and M. Jaeger, "Application of the Adomian Modified Decomposition Method for a Beam With a Single Section Discontinuity Resting on an Elastic Foundation," in *26th International Congress of Sound and Vibration*, ed. M. J. Crocker (Canadian Acoustical Association, 2019).
48. H. Yu, Y. Yang, and Y. Yuan, "Analytical Solution for a Finite Euler–Bernoulli Beam With Single Discontinuity in Section Under Arbitrary Dynamic Loads," *Applied Mathematical Modelling* 60 (2018): 571–580, <https://doi.org/10.1016/j.apm.2018.03.046>.
49. B. Biondi and S. Caddemi, "Euler–Bernoulli Beams With Multiple Singularities in the Flexural Stiffness," *European Journal of Mechanics - A/Solids* 26, no. 5 (2007): 789–809, <https://doi.org/10.1016/j.euromechsol.2006.12.005>.
50. T. Hoang, D. Duhamel, G. Forêt, et al., "Response of a Periodically Supported Beam on a Non-Uniform Viscoelastic Foundation Subject to Moving Loads," in *Proceedings of the Third International Conference on Railway Technology: Research, Development and Maintenance*, ed. J. Pombo and S. Cagliari (Civil-Comp Press, 2016).
51. T. Hoang, D. Duhamel, G. Foret, H. P. Yin, P. Joyez, and R. Caby, "Calculation of Force Distribution for a Periodically Supported Beam Subjected to Moving Loads," *Journal of Sound and Vibration* 388 (2017): 327–338, <https://doi.org/10.1016/j.jsv.2016.10.031>.
52. L.-H. Tran, T. Hoang, G. Foret, and D. Duhamel, "Calculation of the Dynamic Responses of a Railway Track on a Non-Uniform Foundation," *Journal of Vibration and Control* 29, no. 15–16 (2023): 3544–3553, <https://doi.org/10.1177/10775463221099353>.
53. P. Koziol, "Analytical Modelling of Rail Track to Account for Non-linear Properties of Structure," in *MATEC Web of Conferences*, vol. 262 (EDP Sciences, 2019), 11005, <https://doi.org/10.1051/mateconf/201926211005>.

Supporting Information

Additional supporting information can be found online in the Supporting Information section.

Appendix A

For an Euler–Bernoulli beam on a (possibly unbounded) interval (a, b) , with constant foundation stiffness k , we have the ordinary differential equation for the static deformation

$$EI \frac{d^4 y}{dx^4} + ky = 0 \quad (\text{A1})$$

A general solution to this equation can be found using the method of undetermined coefficients.

We begin by assuming a solution of the form $y = e^{rx}$. Substituting into (A1), and comparing coefficients gives the characteristic equation

$$EI r^4 + k = 0 \quad (\text{A2})$$

which has four solutions

$$r = \sqrt[4]{k/EI} m_j, \quad j = 1, 2, 3, 4 \quad (\text{A3})$$

where

$$m_1 = \frac{1}{\sqrt{2}}(1 + i) \quad (\text{A4a})$$

$$m_2 = \frac{1}{\sqrt{2}}(1 - i) \quad (\text{A4b})$$

$$m_3 = \frac{1}{\sqrt{2}}(-1 + i) \quad (\text{A4c})$$

$$m_4 = \frac{1}{\sqrt{2}}(-1 - i) \quad (\text{A4d})$$

and $i = \sqrt{-1}$.

Since (A1) is linear, we construct the general solution by superposition. Doing so gives the general solution

$$y = c_1 e^{\sqrt[4]{k/EI} m_1 x} + c_2 e^{\sqrt[4]{k/EI} m_2 x} + c_3 e^{\sqrt[4]{k/EI} m_3 x} + c_4 e^{\sqrt[4]{k/EI} m_4 x} \quad (\text{A5})$$

The undetermined complex coefficients c_j can then be found by enforcing boundary conditions. Most notably, in the context of this paper, if the interval (a, b) is unbounded below, then to prevent the deformation y becoming unbounded, we must have $c_3 = c_4 = 0$. Likewise, if the interval is unbounded above, we must have $c_1 = c_2 = 0$.

We form the general solution across the entire beam by combining disjoint sub-intervals. Doing so, and relabelling indices, yields

$$y(x) = \begin{cases} c_1 e^{\sqrt[4]{k_0/EI} m_3 x} + c_2 e^{\sqrt[4]{k_0/EI} m_4 x} & x < x_1, \\ \sum_{j=1}^4 c_{j+2} e^{\sqrt[4]{k_1/EI} m_j x} & x_1 < x < x_2, \\ \vdots & \\ \sum_{j=1}^4 c_{\eta-4+j} e^{\sqrt[4]{k_{\eta-1}/EI} m_j x} & x_{\eta-1} < x < x_\eta, \\ c_{4\eta-1} e^{\sqrt[4]{k_\eta/EI} m_1 x} + c_{4\eta} e^{\sqrt[4]{k_\eta/EI} m_2 x} & x_\eta < x \end{cases} \quad (\text{A6})$$

where x_i , $i = 1, \dots, \eta$, are the locations of the boundaries between segments, and k_i are the stiffnesses in these segments.

Appendix B

Consider a beam, as set up in this paper, with a point force at x_p and also a transition zone, from k_1 to k_2 at this point. Integrating the governing equation, (6), across this point gives

$$\int_{x_p^-}^{x_p^+} EI \frac{d^4 y}{dx^4} + k(x)y dx = \int_{x_p^-}^{x_p^+} P \delta(x - x_p) dx \quad (\text{B1a})$$

$$EI \left[\frac{d^4 y}{dx^4} \right]_{x_p^-}^{x_p^+} + \int_{x_p^-}^{x_p^+} k_1 y dx + \int_{x_p^-}^{x_p^+} k_2 y dx = P \quad (\text{B1b})$$

By the continuity of y , we can reduce this to simply

$$\frac{d^3 y}{dx^3} \Big|_{x_p} = \frac{P}{EI} \quad (\text{B2})$$

which, noting that this extends to the case of no transition zone by taking $k_1 = k_2$, completes the boundary conditions at a point-force.

Appendix C

The equations arising from the implementation of boundary conditions described in this paper are as follows. At boundaries x_i for $i = 2, \dots, \eta - 1$, we have

$$\sum_{j=1}^4 c_{4i-6+j} e^{\sqrt[4]{k_{i-1}/EI} m_j x_i} - \sum_{j=1}^4 c_{4i-2+j} e^{\sqrt[4]{k_i/EI} m_j x_i} = 0 \quad (\text{B3a})$$

$$\sum_{j=1}^4 c_{4i-6+j} \sqrt[4]{k_{i-1}/EI} m_j e^{\sqrt[4]{k_{i-1}/EI} m_j x_i} - \sum_{j=1}^4 c_{4i-2+j} \sqrt[4]{k_i/EI} m_j e^{\sqrt[4]{k_i/EI} m_j x_i} = 0 \quad (\text{B3b})$$

$$\sum_{j=1}^4 c_{4i-6+j} \left(\sqrt[4]{k_{i-1}/EI} m_j \right)^2 e^{\sqrt[4]{k_{i-1}/EI} m_j x_i} - \sum_{j=1}^4 c_{4i-2+j} \left(\sqrt[4]{k_i/EI} m_j \right)^2 e^{\sqrt[4]{k_i/EI} m_j x_i} = 0 \quad (\text{B3c})$$

$$\sum_{j=1}^4 c_{4i-6+j} \left(\sqrt[4]{k_{i-1}/EI} m_j \right)^3 e^{\sqrt[4]{k_{i-1}/EI} m_j x_i} - \sum_{j=1}^4 c_{4i-2+j} \left(\sqrt[4]{k_i/EI} m_j \right)^3 e^{\sqrt[4]{k_i/EI} m_j x_i} = \begin{cases} -P/EI, & x_i = x_p, \\ 0, & \text{otherwise} \end{cases} \quad (\text{B3d})$$

At the first boundary, x_1 , we have

$$\sum_{j=1}^2 c_j e^{\sqrt[4]{k_0/EI} m_{j+2} x_1} - \sum_{j=1}^4 c_{2+j} e^{\sqrt[4]{k_1/EI} m_j x_1} = 0 \quad (\text{B4a})$$

$$\sum_{j=1}^2 c_j \sqrt[4]{k_0/EI} m_{j+2} e^{\sqrt[4]{k_0/EI} m_{j+2} x_1} - \sum_{j=1}^4 c_{2+j} \sqrt[4]{k_1/EI} m_j e^{\sqrt[4]{k_1/EI} m_j x_1} = 0 \quad (\text{B4b})$$

$$\sum_{j=1}^2 c_j \left(\sqrt[4]{k_0/EI} m_{j+2} \right)^2 e^{\sqrt[4]{k_0/EI} m_{j+2} x_1} - \sum_{j=1}^4 c_{2+j} \left(\sqrt[4]{k_1/EI} m_j \right)^2 e^{\sqrt[4]{k_1/EI} m_j x_1} = 0 \quad (\text{B4c})$$

$$\sum_{j=1}^2 c_j \left(\sqrt[4]{k_{i-1}/EI} m_{j+2} \right)^3 e^{\sqrt[4]{k_{i-1}/EI} m_{j+2} x_i} - \sum_{j=1}^4 c_{2+j} \left(\sqrt[4]{k_i/EI} m_j \right)^3 e^{\sqrt[4]{k_i/EI} m_j x_i} = \begin{cases} -P/EI, & x_i = x_p, \\ 0, & \text{otherwise} \end{cases} \quad (\text{B4d})$$

At the final boundary, x_η , we have

$$\sum_{j=1}^4 c_{4\eta-6+j} e^{\sqrt[4]{k_{\eta-1}/EI} m_j x_\eta} - \sum_{j=1}^2 c_{4\eta-2+j} e^{\sqrt[4]{k_\eta/EI} m_j x_\eta} = 0 \quad (\text{B5a})$$

$$\sum_{j=1}^4 c_{4\eta-6+j} \sqrt[4]{k_{\eta-1}/EI} m_j e^{\sqrt[4]{k_{\eta-1}/EI} m_j x_\eta} - \sum_{j=1}^2 c_{4\eta-2+j} \sqrt[4]{k_\eta/EI} m_j e^{\sqrt[4]{k_\eta/EI} m_j x_\eta} = 0 \quad (\text{B5b})$$

$$\sum_{j=1}^4 c_{4\eta-6+j} \left(\sqrt[4]{k_{\eta-1}/EI} m_j \right)^2 e^{\sqrt[4]{k_{\eta-1}/EI} m_j x_\eta} - \sum_{j=1}^2 c_{4\eta-2+j} \left(\sqrt[4]{k_\eta/EI} m_j \right)^2 e^{\sqrt[4]{k_\eta/EI} m_j x_\eta} = 0 \quad (\text{B5c})$$

$$\sum_{j=1}^4 c_{4\eta-6+j} \left(\sqrt[4]{k_{\eta-1}/EI} m_j \right)^3 e^{\sqrt[4]{k_{\eta-1}/EI} m_j x_\eta} - \sum_{j=1}^2 c_{4\eta-2+j} \left(\sqrt[4]{k_\eta/EI} m_j \right)^3 e^{\sqrt[4]{k_\eta/EI} m_j x_\eta} = \begin{cases} -P/EI, & x_\eta = x_p, \\ 0, & \text{otherwise} \end{cases} \quad (\text{B5d})$$

In the case that there is only one boundary, that is, $\eta = 1$, the system of equations is given by

$$\sum_{j=1}^2 c_j e^{\sqrt[4]{k_0/EI} m_{j+2} x_1} - \sum_{j=1}^2 c_{2+j} e^{\sqrt[4]{k_1/EI} m_j x_1} = 0 \quad (\text{B6a})$$

$$\sum_{j=1}^2 c_j \sqrt[4]{k_0/EI} m_{j+2} e^{\sqrt[4]{k_0/EI} m_{j+2} x_1} - \sum_{j=1}^2 c_{2+j} \sqrt[4]{k_1/EI} m_j e^{\sqrt[4]{k_1/EI} m_j x_1} = 0 \quad (\text{B6b})$$

$$\sum_{j=1}^2 c_j \left(\sqrt[4]{k_0/EI} m_{j+2} \right)^2 e^{\sqrt[4]{k_0/EI} m_{j+2} x_1} - \sum_{j=1}^2 c_{2+j} \left(\sqrt[4]{k_1/EI} m_j \right)^2 e^{\sqrt[4]{k_1/EI} m_j x_1} = 0 \quad (\text{B6c})$$

$$\sum_{j=1}^2 c_j \left(\sqrt[4]{k_{i-1}/EI} m_{j+2} \right)^3 e^{\sqrt[4]{k_{i-1}/EI} m_{j+2} x_i} - \sum_{j=1}^2 c_{2+j} \left(\sqrt[4]{k_i/EI} m_j \right)^3 e^{\sqrt[4]{k_i/EI} m_j x_i} = -P/EI \quad (\text{B6d})$$